Supplementary Information

Dual-Function Pt/Ir-Doped CdS Catalysts: Defect Engineering for Visible-Light HMF Photo Oxidation and Hydrogen Evolution Reaction

Sunyoung Hwang,[a,†] Yerim Kim,[a,†] Yoonbeen Kang,[b,†] Jeonghyeon Kim,[c,†] Heewon Kim,[a] Yerin Bang,[d] Seojin Baek,[b] Jaeyoon Baik,[e] Seung-Ryong Kwon,[d] Sang-Yong Ju,[b,] Seol Baek,[a,*] and Hangil Lee[a,*]*

[a]Department of Chemistry, Sookmyung Women's University, Seoul 04310, Republic of Korea

[b]Department of Chemistry, Yonsei University, Seoul 03722, Republic of Korea

[c]Hydrogen Fuel Cell Research Center, Korea Institute of Science and Technology (KIST), Seoul 02792, Republic of Korea

[d]Department of Chemistry, Research Institute of Molecular Alchemy, Gyeongsang National University, Jinju 52828, Republic of Korea

[e]Beamline Research Division, Pohang Accelerator Laboratory (PAL), Pohang 37673, Republic of Korea

†These authors contributed equally to this work.

*To whom correspondence should be addressed; E-mail: sbaek@sookmyung.ac.kr, syju@yonsei.ac.kr, easyscan@sookmyung.ac.kr

Table S1. Binding energies obtained from XPS analysis for the four CdS NPs.

Samples	Binding energy (eV)		
	Cd 3*d* CdS/CdS_{1-x}	S 2*p* CdS/MS	M
CdS	404.8/0.0	161.1/0.0	
Li_{dp}-CdS	404.8/0.0	161.1/0.0	Li 1*s*: 55.6
Ir_{dp}-CdS	405.0/404.1	160.85/160.35	Ir $4f_{7/2}$: 64.95
Pt_{dp}-CdS	404.95/404.05	160.0/160.30	Pt $4f_{7/2}$: 72.1

Table S2. Bandgap, E_F energy, and work function obtained from DRS and XPS analysis for the four CdS NPs.

Samples	Bandgap (eV)	E_F (eV)	Work function (eV)
CdS	2.30	1.75	4.45
Li_{dp}-CdS	2.34	1.72	4.30
Ir_{dp}-CdS	2.24	1.65	4.60
Pt_{dp}-CdS	2.21	1.60	4.70

Table S3. Comparison of Ir_{dp}-CdS with representative recently reported photocatalytic systems for HMF oxidation in aqueous media.

Catalyst	Light Source & Power	Base (additive) / Reaction time / HMF Conc.	Target Product	Performance (HMF Conv. / Sel. or Yield)	Ref.
Au/ZnO_{DP-H}	300W Xe lamp (λ>420 nm)	Na_2CO_3 / 5 h / HMF conc.: 31.7 mM	FDCA	HMF Conv.: 55.6% FDCA Yield: 53.9% Sel.: 96.9%	[1]
UCNT/Pt (3 wt.%)	300W Xe lamp (λ≥420 nm)	Base free / 5 h / HMF conc.: 10 mM	DFF	DFF Sel.: 95%	[2]
α-Fe_2O_3/$Zn_{0.5}Cd_{0.5}S$	12W LED (413 nm)	(Air or Ar) / 24–32 h HMF conc.: 100 mM	DFF FDCA	HMF Conv.: 75%, DFF Sel. (24 h, under Ar): 99% HMF Conv.: 99%, FDCA Sel. (32 h, air) : 85%	[3]
CdS@MXene	LED (λ>420 nm)	Base free / 6 h / HMF conc.: 1 mM	DFF	HMF Conv.: 63.89% DFF Sel: 91.63% DFF Yield 58.49%	[4]
CdS/WO_3	6W LED (445 nm)	Base free / 24 h HMF conc.: 25 mM	FDCA	HMF Conv: >97% FDCA Yield: 61% (24h)	[5]
Ir_{dp}-CdS	6W LED (445 nm)	Base free / 24 h HMF conc.: 25 mM	FDCA	HMF Conv: >95% FDCA Yield: 59% (24h)	This Work

Table S4. Comparison of the electrocatalytic activity with other previously reported CdS-based catalysts for HER.

Catalysts	Tafel slope ($mV \cdot dec^{-1}$)	Overpotential (mV)	Solution	Ref.
CdS_{1-x}	131.6	401 (η_{10})	1 M KOH	[6]
20 wt % CdS_{1-x} in WO_{3-x}	61.9	191 (η_{10})	1 M KOH	[6]
ZnS/CdS	313.6	299 (η_{10})	0.5 M H_2SO_4	[7]
VS_2/ZnS/CdS	74.4	86 (η_{10})	0.5 M H_2SO_4	[7]
CdS	151	334 (η_{10})	1 M KOH	[8]
CdS-V_2O_5	104	238 (η_{10})	1 M KOH	[8]
CdS-V_2O_5/ g-C_3N_4	63	202 (η_{10})	1 M KOH	[8]
CdS	111	225 (η_{10})	1 M KOH	[9]
CdS/MIL-101(Fe) (3:1)	47	108 (η_{10})	1 M KOH	[9]
Ir_{dp}-CdS	57.5	198.3 (η_1)	1 M KOH	This Work
Pt_{dp}-CdS	128.8	575.8 (η_1)	1 M KOH	This Work

Fig. S1 (a) Wide-angle XRD patterns and (b) Corresponding enlarged XRD view of the selected region for CdS (orange), Li_{dp}-CdS (green), Ir_{dp}-CdS (red), and Pt_{dp}-CdS NPs (blue).

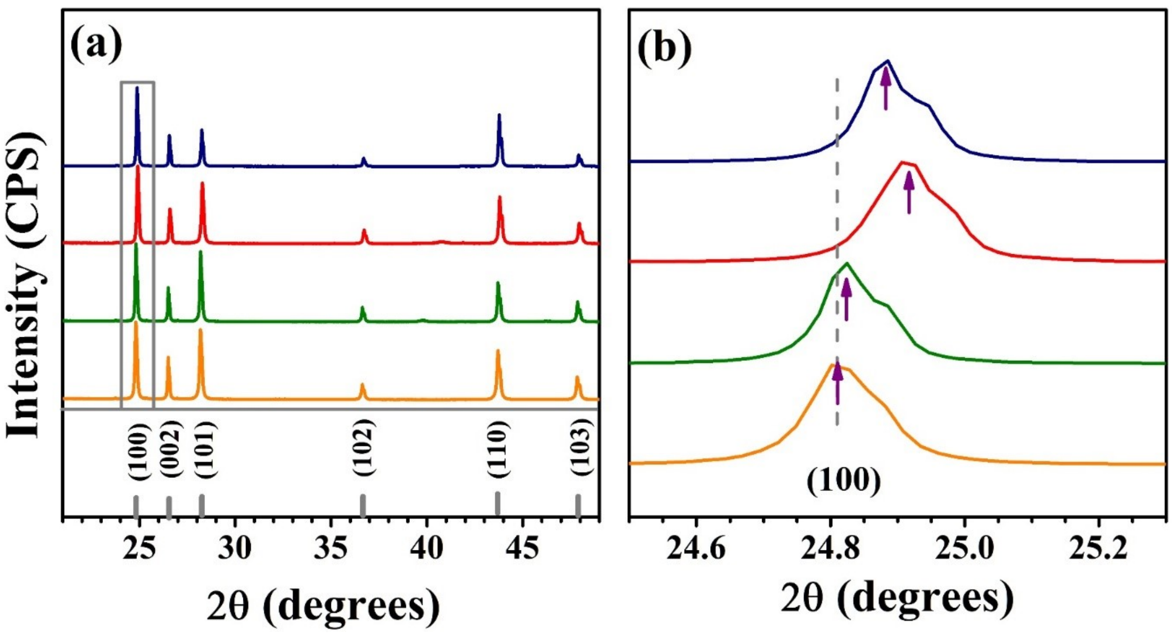

Fig. S2 (a) Zoom-in Raman spectra, (b) Photocurrents generated by CdS (black), Li_{dp}-CdS (green), Ir_{dp}-CdS (red), and Pt_{dp}-CdS (blue) NPs in the presence of Na_2SO_3 (0.025 M) as a hole scavenging agent.

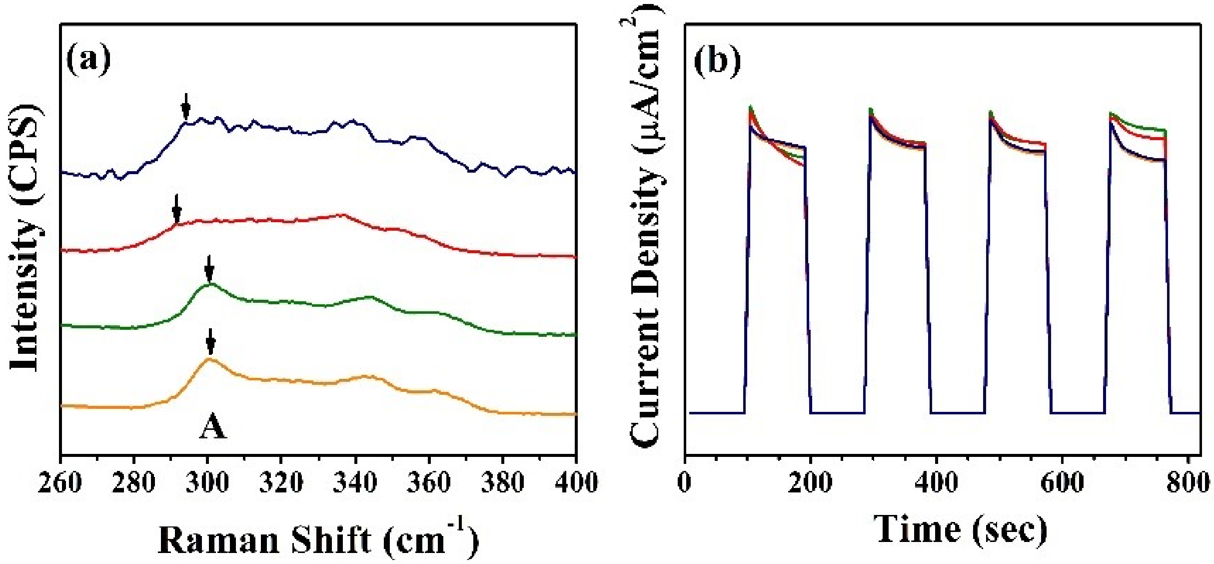

Fig. S3 (a) UV-Vis DRS spectra, (b) Work function measurements, and (c) Valence band spectra of CdS (orange), Li_{dp}-CdS (green), Ir_{dp}-CdS (red), and Pt_{dp}-CdS (blue) NPs.

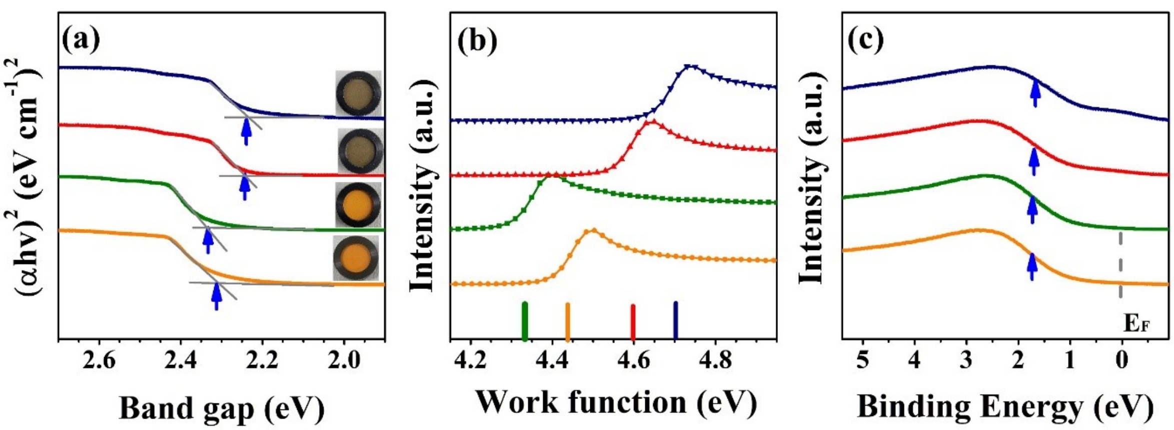

Fig. S4 LC-MS spectra of the four CdS NPs.

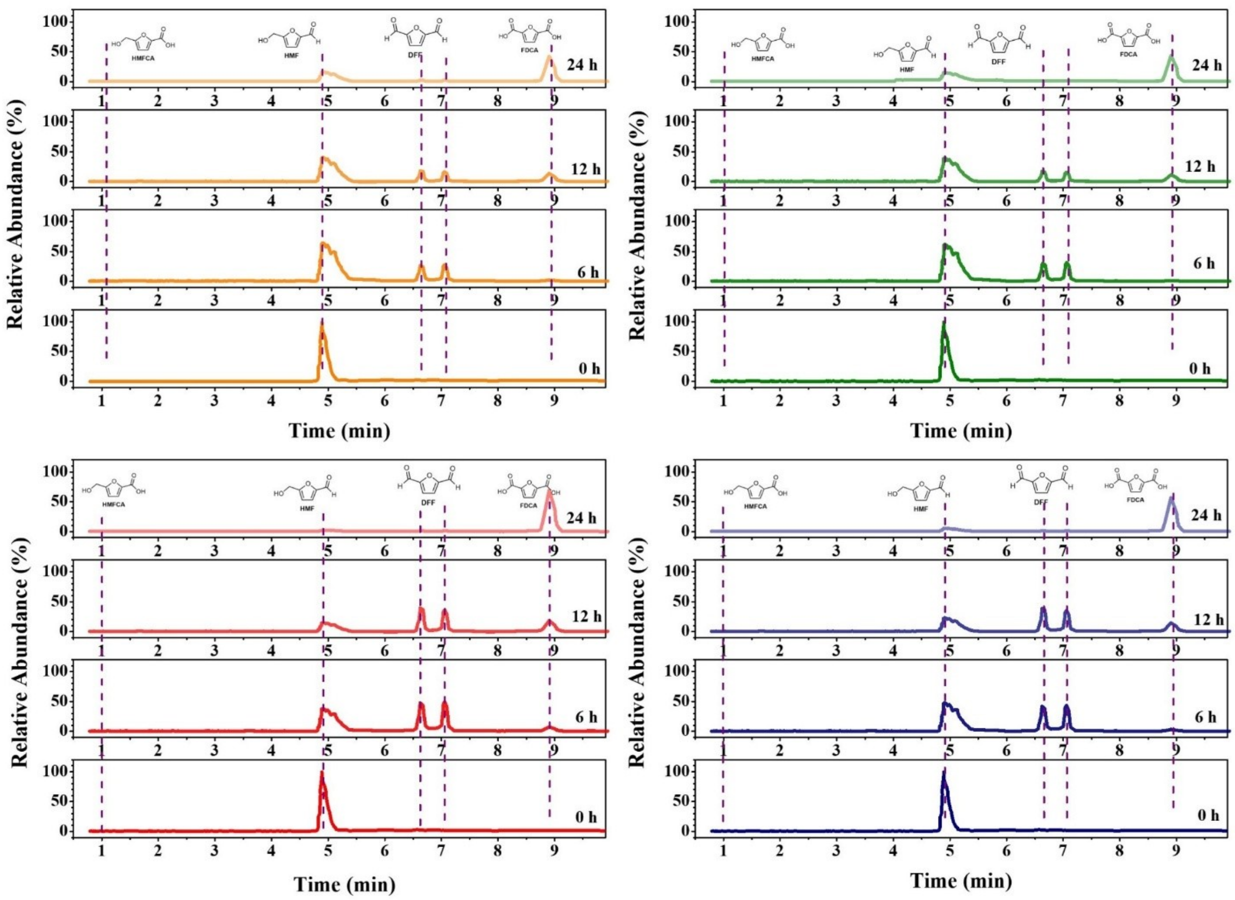

Fig. S5 EPR spectra of CdS and Ir_{dp}-CdS NPs using (a) DMPO and (b) TMP as $^{\bullet}O_2^{-}$-trapping agent and $^{1}O_2$-trapping agents.

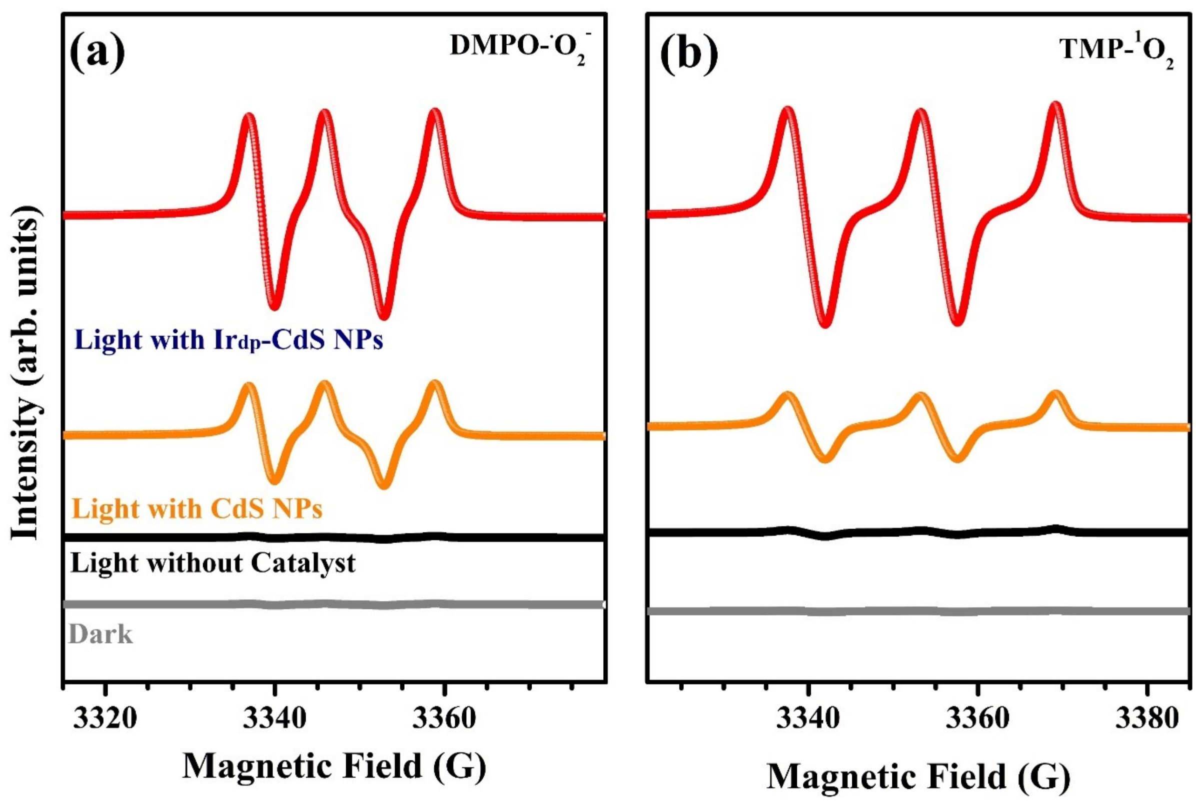

Fig. S6 Conversion rate of HMF and FDCA yields in the presence of 1, 3, 5, and 7 wt.% doping of Li (a and d), Ir (b and e), and Pt (c and f) ions.

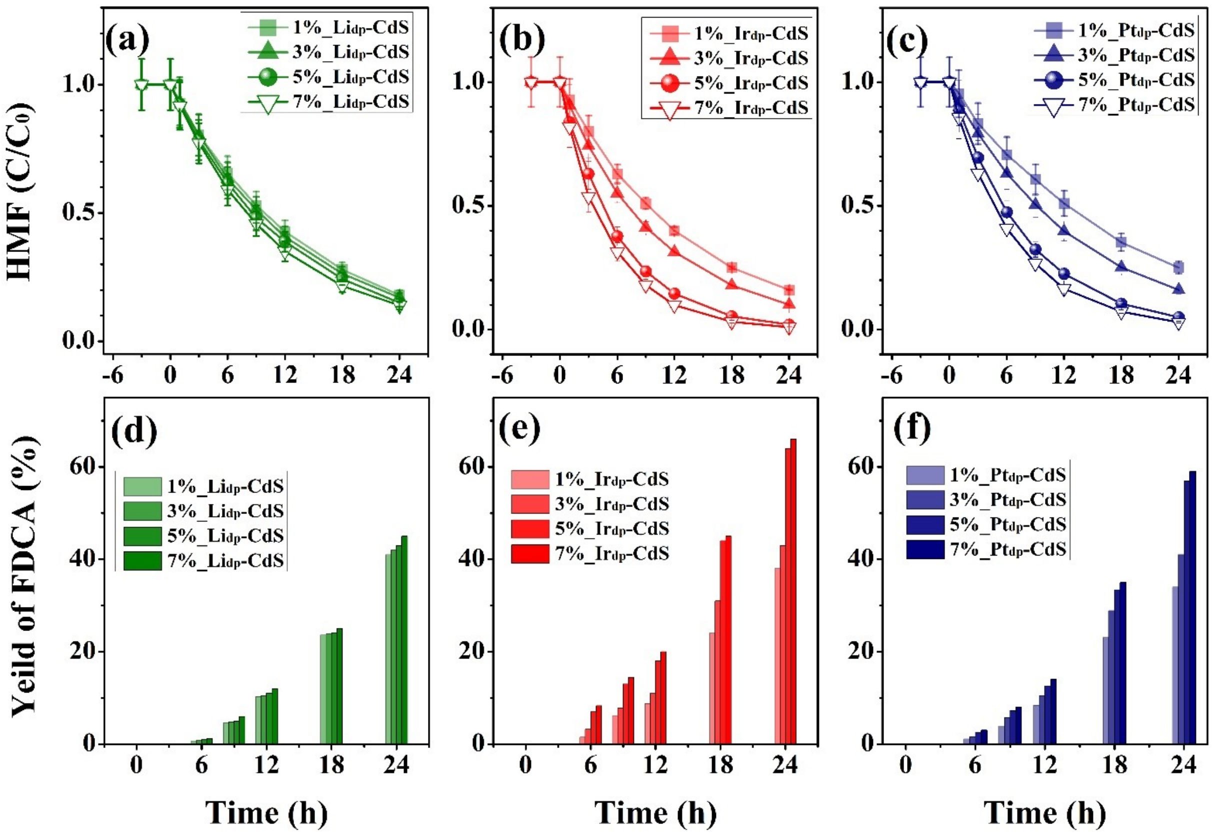

Fig. S7 Cyclic photocatalytic HMF-decomposition data for CdS (orange), Li_{dp}-CdS (green), Ir_{dp}-CdS (red), and Pt_{dp}-CdS (blue) NPs at 445 nm.

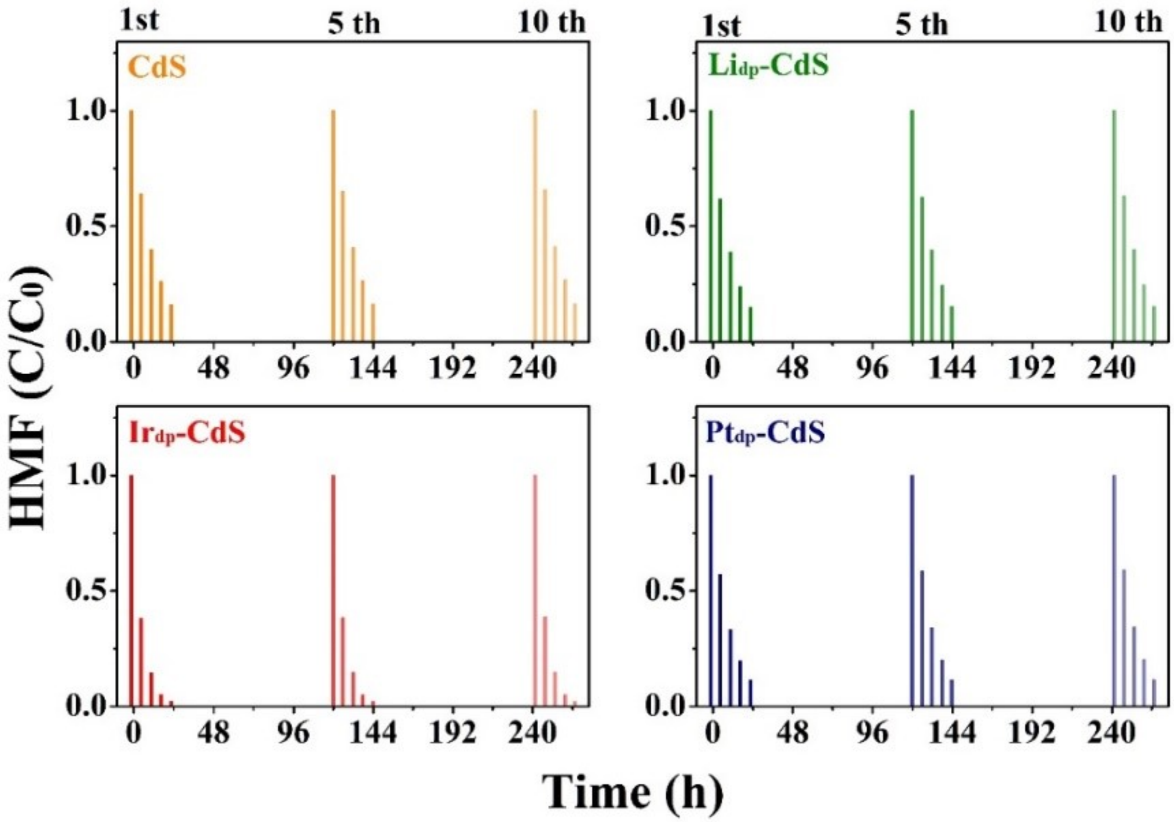

Fig. S8 XRD patterns (a) before and (b) after PCR experiments for CdS (orange), Li_{dp}-CdS (green), Ir_{dp}-CdS (red), and Pt_{dp}-CdS (blue) NPs.

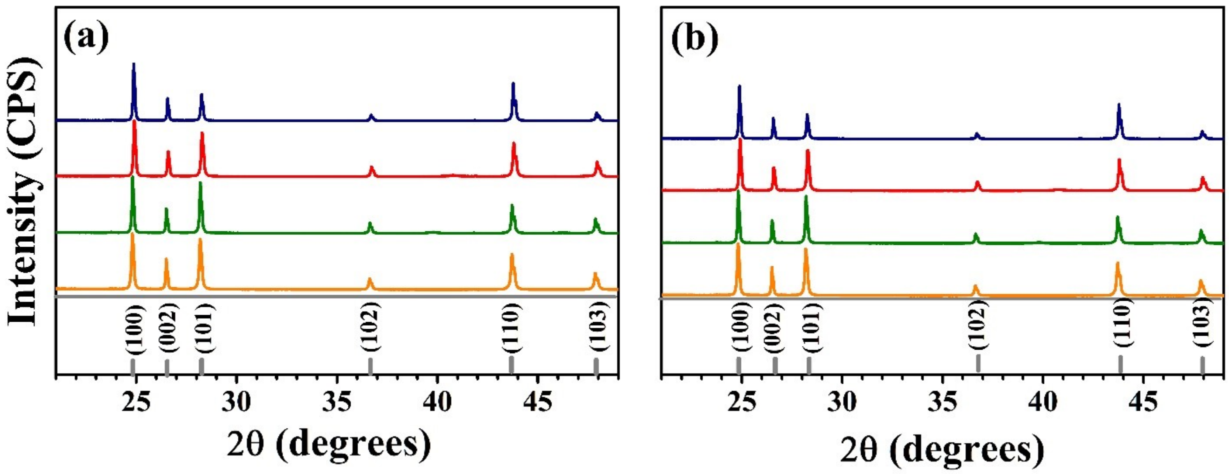

Fig. S9 XPS spectra of (a–e) before and (f–j) after PCR experiments for CdS (orange), Li_{dp}-CdS (green), Ir_{dp}-CdS (red), and Pt_{dp}-CdS (blue) NPs.

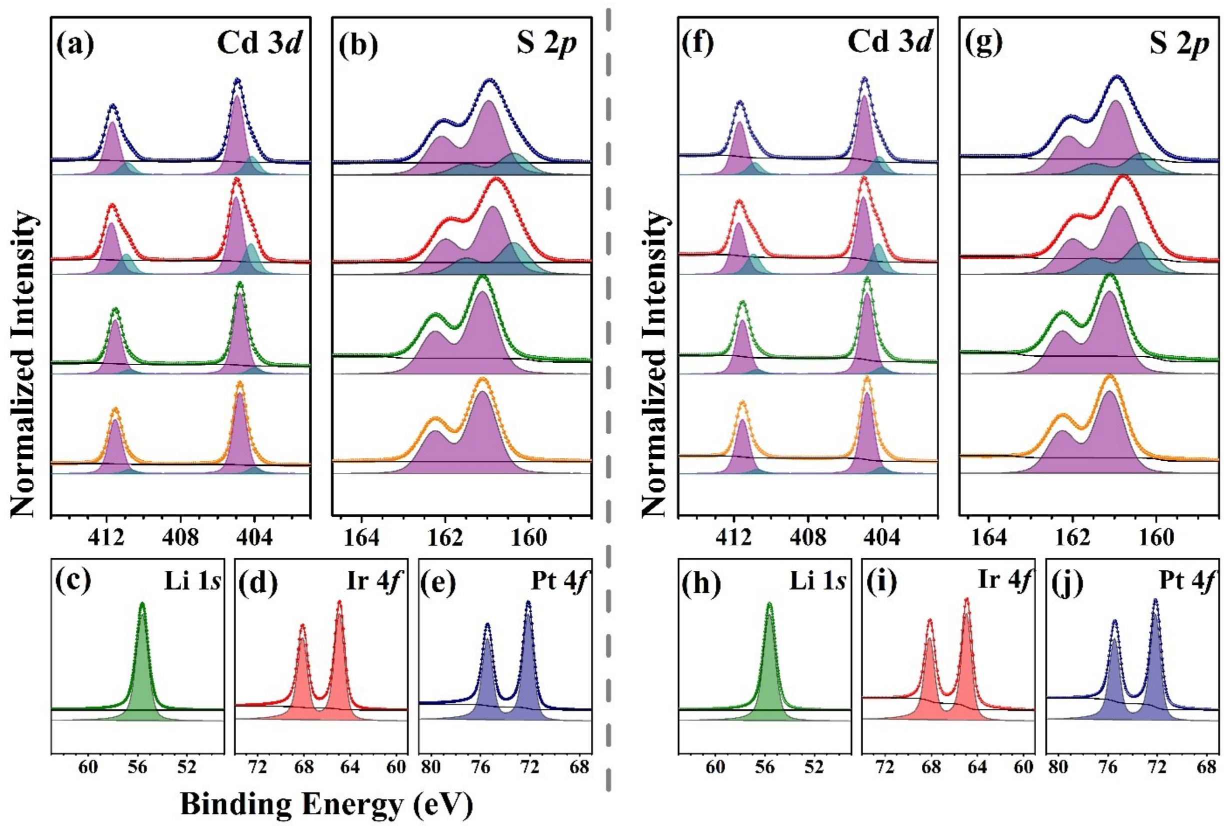

Fig. S10 (a) LSV curve of Pt_{dp}-CdS NPs in 1 M KOH. Marked points indicate the overpotential at which bubble behavior was observed. (b) Corresponding optical images showing bubble dynamics at selected overpotentials of 0, −0.22, −0.5, and −0.72 V.

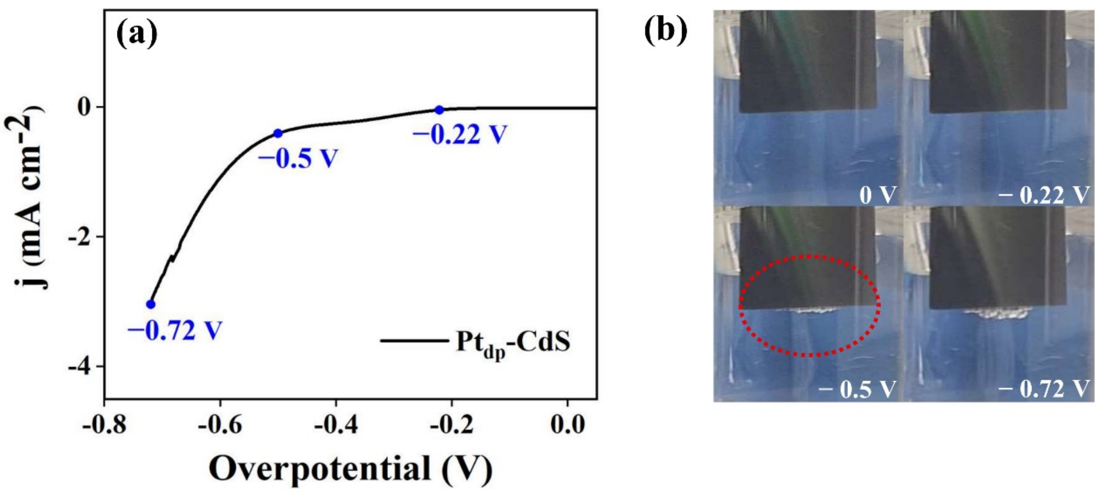

Fig. S11 (a) LSV curve of Ir_{dp}-CdS NPs in 1 M KOH. Marked points indicate the overpotential at which bubble behavior was observed. (b) Corresponding optical images showing bubble dynamics at selected overpotentials of 0, −0.22, −0.5, and −0.72 V.

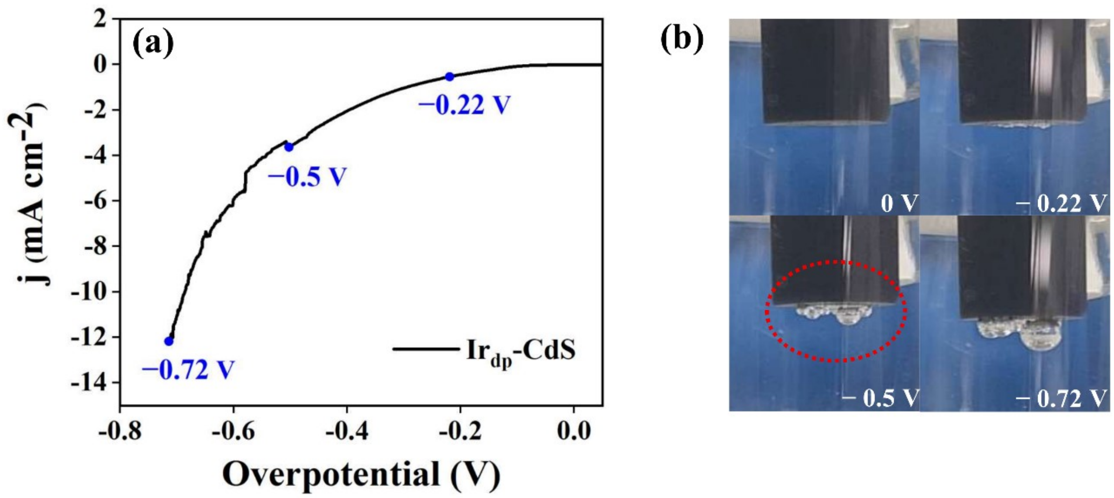

Fig. S12 (a) LSV curve of Pt_{dp}-CdS NPs in 1 M KOH. Marked points indicate the current density at which bubble behavior was observed. (b) Corresponding optical images showing bubble dynamics at selected current densities of 0, −0.04, −0.40, and −3.05 mA·cm^{-2}.

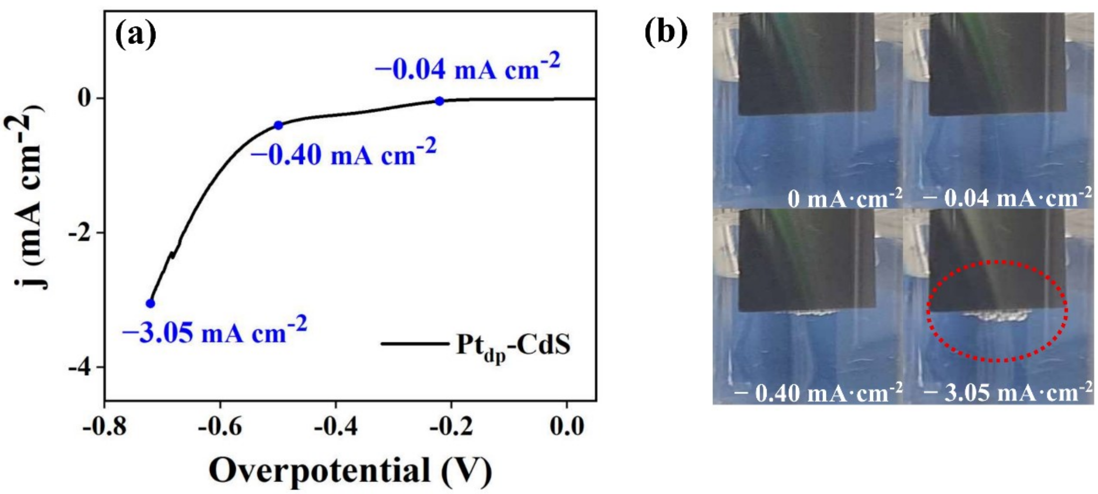

Fig. S13 (a) LSV curve of Ir_{dp}-CdS in 1 M KOH. Marked points indicate the current density at which bubble behavior was observed. (b) Corresponding optical images showing bubble dynamics at selected current densities of 0, −0.04, −0.40, and −3.05 $mA \cdot cm^{-2}$.

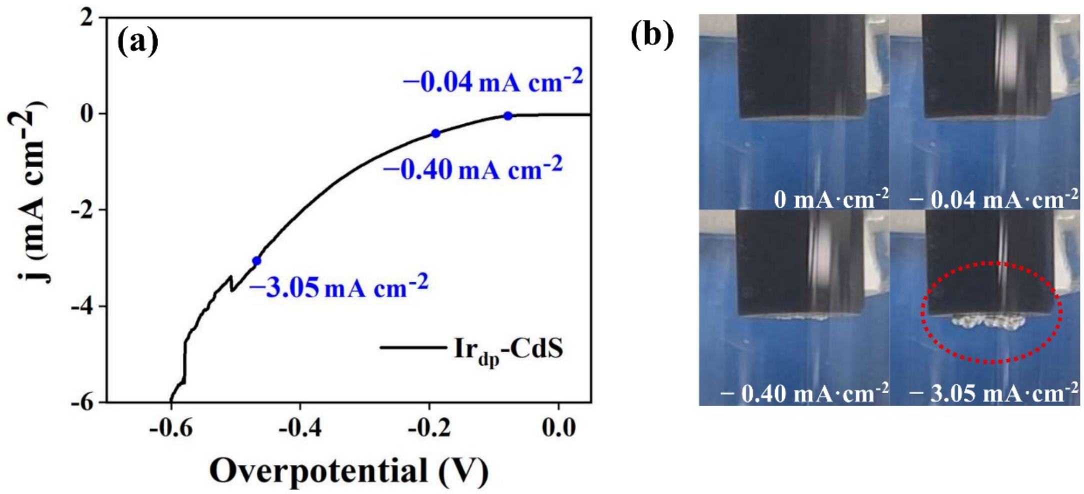

References

[1] P. Zhu, W. Zhang, Q. Li, H. Xia, *ACS Sustain. Chem. Eng.* 2022, **10**, 8778–8787.

[2] X. Bao, M. Liu, Z. Wang, D. Dai, P. Wang, H. Cheng, Y. Liu, Z. Zheng, Y. Dai, B. Huang, *ACS Catal.* 2022, **12**, 1919–1929.

[3] Y. Wang, C. Cai, *ACS Catal.* 2025, **15**, 3451–3463.

[4] C. Zhang, P. Zhan, H. Shan, W. Ren, Y. Liu, X. Liu, S. Zheng, Z. Liao, D. Cai, P. Qin, *Chem. Eng. J.* 2025, **506**, 159946.

[5] H. Yu, D. T. Hoang, H. S. Kim, H. Lee, *J. Mater. Chem. A,* 2025, **13**, 6049-6058.

[6] M. J. S. Mohamed, M. A. Gondal, M. Hassan, M. A. Almessiere, A. A. Tahir and A. Roy, *ACS Omega,* 2023, **8,** 33332–33341.

[7] P. V. Shinde, D. S. Gavali, R. Thapa, M. K. Singh and C. S. Rout, *AIP Advances,* 2021, **11,** 105010.

[8] T. Munawar, A. Bashir, F. Iqbal, M. Rafaqat, C. Guo, M. Zhiani, C. Zhao, Y. Tong, S. A. Khan and M. Koc, *Fuel,* 2025, **385,** 134100.

[9] M. Ali, E. Pervaiz and U. Sohail, *Energy & Fuels,* 2023, **37,** 7919–7926.